

Application of the Stabilization Method to Temporary Anion States of π -Ligand Transition-Metal Carbonyls in Density Functional Theory

Hsiu-Yao Cheng,* Jung-Tzu Chang, and Chun-Chi Shih

Department of Chemistry, Tunghai University, Taichung 40704, Taiwan

Received: October 24, 2009; Revised Manuscript Received: January 26, 2010

In this paper, density functional theory is used to investigate (benzene)chromium tricarbonyl, (cyclopentadienyl)manganese tricarbonyl, (1,3-butadiene)iron tricarbonyl, and (cyclopentadienyl)cobalt dicarbonyl. For the energies of low-lying temporary anion states, the stabilized Koopmans-based (S-KB) and stabilized Koopmans theorem (S-KT) methods are adopted. Stabilization is accomplished by varying the exponents of appropriate diffuse functions. Results indicate that the calculations of S-KB using PBEPBE and S-KT using CAM-B3LYP are able to yield energies of temporary anion states in good agreement with the experimental values. Furthermore, the ionization potentials can be determined accurately via the Koopmans-based (KB) PBEPBE method.

1. Introduction

The carbonyl-containing transition-metal complexes have aroused both theoretical and experimental interest due to their importance in organic synthesis, catalytic chemistry, and application in potential nonlinear optics.^{1–4} The determination of ionization potentials (IPs), electron affinities (EAs), and frontier molecular orbitals are imperative in understanding the bonding, catalytic properties, and nonlinear optical activity of this class of transition-metal complexes. In general, the IPs and EAs can be determined by means of photoelectron spectroscopy (PES)⁵ and electron transmission spectroscopy (ETS),^{6,7} respectively. However, the assignment of the photoelectron spectra was not accurate in most of the recently studied organometallic systems, as mentioned in the work of Gengeliczki et al.⁸ Furthermore, theoretical investigation of the unoccupied orbitals of organometallic complexes is also scarce.

In the theoretical prediction of IPs and EAs, the Koopmans theorem (KT)⁹ approximation using Hartree–Fock (HF) or Kohn–Sham (KS) orbital energies is usually adopted. The IPs and EAs in the KT approximation are associated with the negatives of the energies of the filled and unfilled orbitals, respectively. However, it neglects relaxation and correlation effects. Meanwhile, the KT approximation does not mean that any orbital energy may be considered an approximate electron binding energy. Some one-electron equations give physically meaningful orbital energies. Others may not. In using the KT approximation, most density functional theory (DFT)¹⁰ potentials will not yield asymptotic behavior properly.^{11,12} Various schemes have been devised for long-range correction (LRC). For instance, Tozer and co-workers have proposed an alternative Koopmans-based (KB) approximation based on the consideration of the integer discontinuity (Δ_{xc}) in the exact exchange–correlation potential.^{12–17} However, for species with negative EAs, the temporary anion is unstable with respect to electron detachment. Thus, the unfilled orbitals are prone to collapse onto approximations of continuum functions called orthogonalized discretized continuum (ODC)^{18–21} when large basis sets are used. Therefore,

the energy calculations of temporary anion states using both the KT and KB approaches are not considered definitive.

The stabilization method proposed by Taylor and co-workers^{22–25} can distinguish the temporary anion orbital solutions from the ODC solutions. The vertical attachment energies (AEs) are associated with the energies of the “stabilized” temporary anion states of the neutral molecules. By combining the stabilization method and consideration of LRC, we have applied the S-KB method (i.e., the stabilization method coupled with KB) in the studies of a series of molecules.^{26,27} Results have indicated that the S-KB approach has yielded an improvement in predicting both the absolute and relative energies of temporary anion states over other approaches.

In this paper, we continue to study prototypical transition-metal carbonyls such as (benzene)chromium tricarbonyl, (cyclopentadienyl)manganese tricarbonyl, (1,3-butadiene)iron tricarbonyl, and (cyclopentadienyl)cobalt dicarbonyl. These important compounds have been studied previously by the multiple scattering $X\alpha$ (MS- $X\alpha$) method.²⁸ However, the stability of the temporary anion states was not established for π -ligand transition-metal carbonyls. In the study of the temporary anion resonances, the S-KB method using the local functional will be adopted first. Then, the S-KT method (i.e., the stabilization method coupled with KT)^{18,19,29} using the LRC functional will be invoked. As to the filled molecular orbitals (MOs), we will apply the KB and KT approximations to the IPs. Finally, the results will be compared with experimental values.

2. Computational Method

The IPs and EAs in the KT approximation can be written as $IP^{KT} \approx -\epsilon_{OMO}$ and $EA^{KT} \approx -\epsilon_{VMO}$, where ϵ_{OMO} and ϵ_{VMO} denote the occupied and virtual molecular orbital energies, respectively. The asymptotic correction of the Koopmans value in the KB approximation is roughly half the integer discontinuity:

$$\frac{\Delta_{xc}}{2} \approx \epsilon_{HOMO} + (E_{N-1} - E_N) \quad (1)$$

Notice that ϵ_{HOMO} is the highest-occupied molecular orbital (HOMO) energy determined from a DFT calculation using a

* Corresponding author. Telephone: 011-886-4-23590248-102. Fax: 011-886-4-23590426. E-mail: hycheng@thu.edu.tw.

local exchange-correlation functional on the neutral system. Here, E_N and E_{N-1} are the total electronic energies of the neutral and cation, respectively. By applying the correction terms $\Delta_{xc}/2$ and $-\Delta_{xc}/2$ to IP^{KT} and EA^{KT} , respectively, the IP and EA in the KB approximation can be written as

$$IP^{KB} \approx -\varepsilon_{OMO} + [\varepsilon_{HOMO} + (E_{N-1} - E_N)] \quad (2)$$

and

$$EA^{KB} \approx -\varepsilon_{VMO} - [\varepsilon_{HOMO} + (E_{N-1} - E_N)] \quad (3)$$

The vertical attachment energy (i.e., $-EA$), can then be represented as

$$AE^{KB} \approx \varepsilon_{VMO} + [\varepsilon_{HOMO} + (E_{N-1} - E_N)] \quad (4)$$

The virtual orbital energy associated with temporary anion state is also known as AE. The AE^{KB} will be denoted as ε_{VMO}^{KB} .

To distinguish the temporary anion state solutions from the virtual ODC ones, the stabilization method is employed. Nine different Gaussian-type basis sets, designated as A1, A2, A3, B1, B2, B4, C1, C2, and C4 are used in our calculations. The convention of designation is explained as follows. For the C and O atoms, the 6-31G+ αp_1 basis set A is formed by augmenting the 6-31G basis set with the diffuse p_1 function multiplied by a scale factor α (denoted by αp_1). The 6-31+G(d)+ αp_2 basis set B is formed by augmenting the 6-31+G(d) basis set with the diffuse αp_2 function. The aug-cc-pvdz+ αp_3 basis set C is formed by augmenting the aug-cc-pvdz basis set with the diffuse αp_3 function. The p_1 , p_2 , and p_3 functions have the exponents of 0.0562, 0.0146, and 0.0135 for the C atom and 0.0900, 0.0282, and 0.0229 for the O atom, respectively. For metal atoms, the following four different Gaussian-type basis sets 1–4 are employed and they are denoted alongside A–C basis sets.

(1) The Wachters+ αd_1 basis set is formed by augmenting the (14s11p6d)/[8s6p4d] all-electron basis set from Wachters³⁰ with the diffuse αd_1 function. The diffuse d_1 functions have the exponents of 0.0304, 0.0351, 0.0378, and 0.0406 for the Cr, Mn, Fe, and Co atoms, respectively.

(2) The akr45+ αd_2 basis set is formed by augmenting the (13s10p5d)/[5s4p2d] akr45 basis set of Rappe, Smedley, and Goddard³¹ with the diffuse αd_2 function. The diffuse d_2 functions have the exponents of 0.0540, 0.0600, 0.0704, and 0.0783 for the Cr, Mn, Fe, and Co atoms, respectively.

(3) The 6-31G+ αd_3 basis set is formed by augmenting the 6-31G basis set with the αd_3 diffuse function. The diffuse d_3 functions have the exponents of 0.1335, 0.1539, 0.1681, and 0.1852 for the Cr, Mn, Fe, and Co atoms, respectively.

(4) The 6-31+G(d)+ αd_1 basis set is formed by augmenting the 6-31+G(d) basis set with the αd_1 diffuse function. In summary, the basis set “Xn” represents both the basis set X (X = A, B, or C) for the C and O atoms and n ($n = 1, 2, 3$, or 4) for the metal atoms. The inclusion of additional diffuse s functions or d polarization functions on C and O and s functions or p functions on metals is found to be unimportant for the energies of resonance states.

As α increases, the ODC solutions may approach the temporary anion state orbital solutions in energy and lead to avoided crossing between the two types of solutions. The stabilization graphs are obtained by plotting the calculated energies (ε_{VMO}^{KB}) as a function of the scale factor α . When the avoided crossing between temporary anion and ODC solutions occurs at their point of closest approach α_{ac} , the energy of the anion shape resonance is taken as the mean value of these two eigenvalues.³²

In the present study, we adopt the (1) local functional via the S-KB method and (2) LRC functional via the S-KT method for the temporary anion states. The local functional chosen is the PBEPBE,³³ which utilizes pure generalized gradient approximation (GGA) functional due to its superior calculated AEs.^{26,27} For the LRC functional, we use CAM-B3LYP,³⁴ wB97XD,³⁵ and LC-wPBE³⁶ functionals. All calculations are performed using the Gaussian 09 program.³⁷ The geometry of $(\eta^6\text{-C}_6\text{H}_6)\text{Cr}(\text{CO})_3$ is optimized under C_{3v} , and the geometries

TABLE 1: Calculated IPs (eV) for $(\eta^6\text{-C}_6\text{H}_6)\text{Cr}(\text{CO})_3$ and $(\eta^5\text{-C}_5\text{H}_5)\text{Mn}(\text{CO})_3$

method	basis set	$(\eta^6\text{-C}_6\text{H}_6)\text{Cr}(\text{CO})_3$				$(\eta^5\text{-C}_5\text{H}_5)\text{Mn}(\text{CO})_3$					
		a ₁	e	e	d ^b /eV	a'	a''	a'	a''	a'	d ^b /eV
KB ^{PBEPBE}	A1	7.38	7.40	10.52	0.08	8.05	8.06	8.35	9.88	9.96	0.08
	A2	7.45	7.46	10.54	0.08	8.13	8.13	8.44	9.88	9.96	0.11
	A3	7.43	7.44	10.56	0.06	8.05	8.06	8.32	9.94	10.03	0.08
	B1	7.57	7.59	10.64	0.13	8.18	8.19	8.48	9.93	10.01	0.13
	B2	7.58	7.59	10.60	0.14	8.22	8.23	8.53	9.92	10.00	0.16
	B4	7.60	7.64	10.69	0.14	8.19	8.19	8.48	9.94	10.03	0.13
	C1	7.56	7.58	10.62	0.13	8.16	8.17	8.45	9.90	9.98	0.12
	C2	7.57	7.60	10.61	0.14	8.19	8.20	8.49	9.90	9.97	0.14
KT ^{CAM-B3LYP}	C4	7.55	7.59	10.63	0.12	8.17	8.17	8.45	9.91	9.98	0.12
	A1	7.33	7.00	10.43	0.26	7.94	7.93	8.53	9.38	9.47	0.34
	B1	8.05	7.75	10.51	0.38	8.13	8.12	8.71	9.49	9.58	0.32
KT ^{wB97XD}	C1	8.02	7.73	10.49	0.37	8.13	8.12	8.68	9.48	9.56	0.32
	A1	7.89	7.59	11.05	0.33	8.51	8.51	9.09	10.00	10.09	0.38
	B1	8.05	7.75	11.08	0.45	8.65	8.64	9.21	10.06	10.15	0.46
KT ^{LC-wPBE}	C1	8.02	7.73	11.05	0.42	8.63	8.62	9.17	10.03	10.12	0.44
	A1	8.45	8.13	11.83	0.96	9.17	9.16	9.72	10.73	10.84	0.99
	B1	8.64	8.32	11.87	1.10	9.33	9.32	9.87	10.81	10.91	1.11
X α^a	C1	8.61	7.30	11.83	0.81	9.31	9.30	9.83	10.77	10.87	1.08
		7.3	7.4	10.8	—	8.0	8.0	8.2	10.1	9.9	—
	expt ^a	7.42	10.70			8.05	8.40	9.90	10.29		

^a The IPs are obtained from previous studies.²⁸ ^b Here d denotes the mean error relative to experimental IP data.

of $(\eta^5\text{-C}_5\text{H}_5)\text{Mn}(\text{CO})_3$, $(\eta^4\text{-C}_4\text{H}_6)\text{Fe}(\text{CO})_3$, and $(\eta^5\text{-C}_5\text{H}_5)\text{Co}(\text{CO})_2$ are optimized under C_s symmetry constraints at the B3LYP/6-31+G(d) level. The overall optimized results of structural parameters are close to the crystallographic data.^{38–40} For $(\eta^6\text{-C}_6\text{H}_6)\text{Cr}(\text{CO})_3$, the optimized bond lengths of Cr–CO and C–O in $\text{Cr}(\text{CO})_3$ and the optimized distance between Cr and the benzene ring are 1.86, 1.16, and 1.74 Å, respectively. For $(\eta^5\text{-C}_5\text{H}_5)\text{Mn}(\text{CO})_3$, the optimized bond lengths of Mn–CO and C–O and the distance of Mn–cyclopentadienyl (Mn–Cp) are 1.81, 1.16, and 1.81 Å, respectively. The optimized bond distances of Co–CO, C–O, and Co–Cp are 1.75, 1.16, and 1.73 Å for $(\eta^5\text{-C}_5\text{H}_5)\text{Co}(\text{CO})_2$, respectively. Finally, for the optimized structure of $(\text{butadiene})\text{Fe}(\text{CO})_3$, one unique CO group is aligned with the open side of the butadiene. The bond lengths of the unique Fe–CO and the other two Fe–CO are 1.79 and 1.80 Å, respectively. The distances between Fe and two inner C atoms of the butadiene and those of Fe and two outer C atoms are 2.08 and 2.13 Å, respectively.

3. Results and Discussion

We perform KB calculations using PBEPBE ($\text{KB}^{\text{PBEPBE}}$) and KT calculations using CAM-B3LYP, wB97XD, and LC-wPBE ($\text{KT}^{\text{CAM-B3LYP}}$, $\text{KT}^{\text{wB97XD}}$, and $\text{KT}^{\text{LC-wPBE}}$) methods on the filled orbitals for transition-metal carbonyls. The calculated IPs for $(\eta^6\text{-C}_6\text{H}_6)\text{Cr}(\text{CO})_3$ and $(\eta^5\text{-C}_5\text{H}_5)\text{Mn}(\text{CO})_3$ are tabulated along with the experimental values in Table 1. In the $\text{KB}^{\text{PBEPBE}}$ method, the first IPs are due to ionization from the a_1 (denoted as $18a_1$) for $(\eta^6\text{-C}_6\text{H}_6)\text{Cr}(\text{CO})_3$ and a' (denoted as $33a'$) for $(\eta^5\text{-C}_5\text{H}_5)\text{Mn}(\text{CO})_3$, respectively. The increasing order of IPs of filled MOs are $a_1 \approx e < e$ for $(\eta^6\text{-C}_6\text{H}_6)\text{Cr}(\text{CO})_3$ and $a' \approx a'' < a' < a'' < a'$ for $(\eta^5\text{-C}_5\text{H}_5)\text{Mn}(\text{CO})_3$. As can be seen from Table 1, the calculated IPs using the $\text{KB}^{\text{PBEPBE}}$ method are in very good agreement with the experimental values. The range of errors is within 0.2 eV for all basis sets. As to the KT calculations, the order of IPs for $(\eta^6\text{-C}_6\text{H}_6)\text{Cr}(\text{CO})_3$, $e < a_1 < e$, is not conformable with that obtained from the $\text{KB}^{\text{PBEPBE}}$ method. The errors for IPs of the $\text{KT}^{\text{CAM-B3LYP}}$, $\text{KT}^{\text{wB97XD}}$, and $\text{KT}^{\text{LC-wPBE}}$ methods are 0.26–0.38, 0.33–0.46, and 0.81–1.11 eV, respectively. They are larger than 0.08–0.13 eV of the $\text{KB}^{\text{PBEPBE}}$ method when the same basis sets are used. Consequently, the $\text{KB}^{\text{PBEPBE}}$ approach has better prediction in IPs than the KT methods. In the $X\alpha$ method, the predicted values are close to those of the $\text{KB}^{\text{PBEPBE}}$ method but the orders of the HOMO–4 (a'') and HOMO–5 (a') orbitals for $(\eta^5\text{-C}_5\text{H}_5)\text{Mn}(\text{CO})_3$ are not conformable with ours.

We then examine the characteristics of MOs using the $\text{KB}^{\text{PBEPBE}}$ method. The correlation diagrams of the frontier MOs of $(\eta^6\text{-C}_6\text{H}_6)\text{Cr}(\text{CO})_3$ and $(\eta^5\text{-C}_5\text{H}_5)\text{Mn}(\text{CO})_3$ are illustrated in Figure 1. Our symmetry in the labeling of the orbital is based on that the z axis is perpendicular to the arene ring. In Figure 1, the ordering of MOs for metals, benzene (Bz), Cp, $(\text{CO})_3$, $\text{Bz}(\text{CO})_3$, and $\text{Cp}(\text{CO})_3$ are estimated using the $(\eta^6\text{-C}_6\text{H}_6)\text{Cr}(\text{CO})_3$ ($(\eta^5\text{-C}_5\text{H}_5)\text{Mn}(\text{CO})_3$) structures by setting up the other atoms as ghost atoms³⁷ via KT. For $(\eta^6\text{-C}_6\text{H}_6)\text{Cr}(\text{CO})_3$, the 3d orbitals of chromium yield a_1 (d_{z^2}), e ($d_{x^2-y^2, xy}$), and e ($d_{xz, yz}$) orbitals in the C_{3v} point group. The π^* orbitals of $(\text{CO})_3$ are of a_1 , e , e , and a_2 symmetries, and those of benzene are of a_1 and e symmetries. For $(\eta^5\text{-C}_5\text{H}_5)\text{Mn}(\text{CO})_3$, the yz plane is defined as the plane of symmetry. The 3d orbitals of manganese yield a' (d_{z^2}), a' ($d_{x^2-y^2}$), a' (d_{yz}), a'' (d_{xy}), and a'' (d_{xz}) orbitals in the C_s point group. The π^* orbitals of $(\text{CO})_3$ are of a' , a'' , a' , a'' , a' , and a'' symmetries, and those of Cp are of a' and a'' symmetries. For both metal carbonyls, 4s or 4p orbitals of metals are mainly core-excited resonances.⁴¹

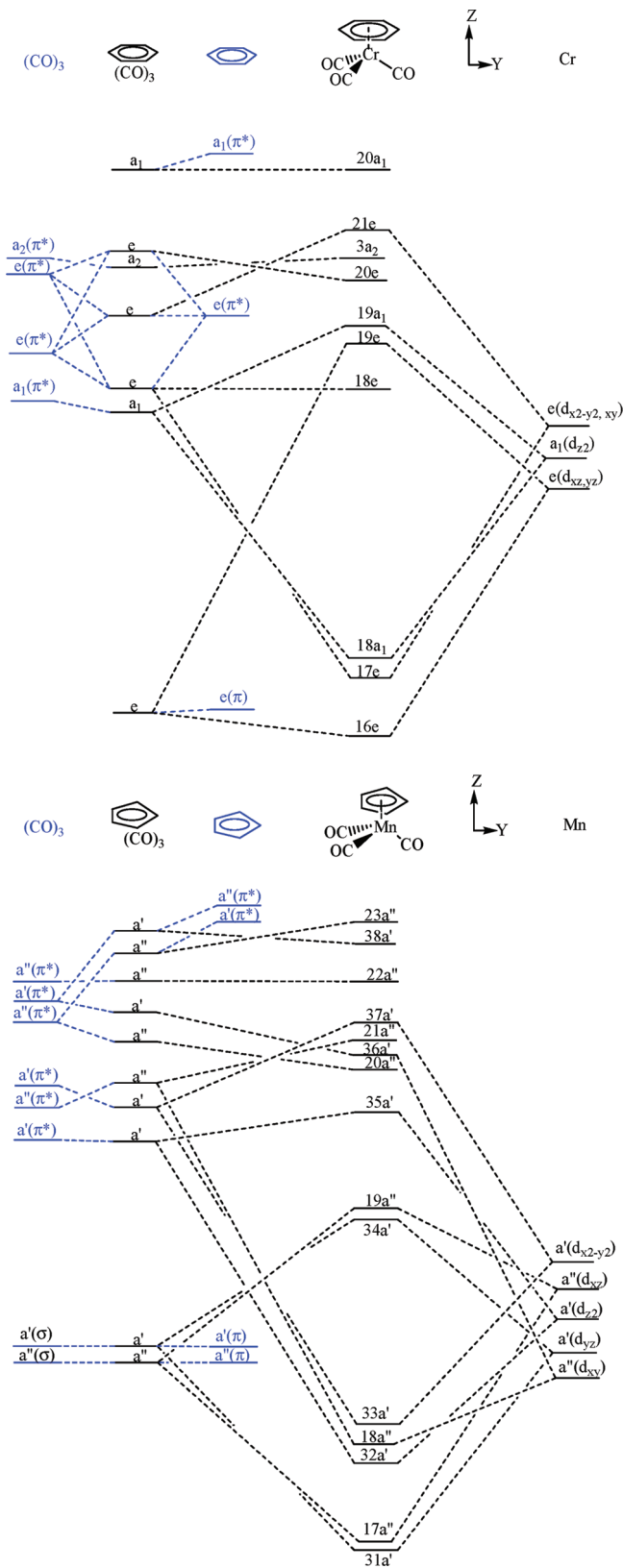


Figure 1. Correlation diagram of the frontier MOs for $(\eta^6\text{-C}_6\text{H}_6)\text{Cr}(\text{CO})_3$ and $(\eta^5\text{-C}_5\text{H}_5)\text{Mn}(\text{CO})_3$.

$(\eta^6\text{-C}_6\text{H}_6)\text{Cr}(\text{CO})_3$ has 18 a_1 , 17 e , and 2 a_2 occupied MOs. Its frontier filled MOs using basis set A1 are illustrated in Figure 2. As indicated in Figure 2, the $18a_1$ orbital is the HOMO. This orbital results from Cr (d_{z^2}) and $(\text{CO})_3$ π^* . The $17e$ orbitals result from the mixing of the benzene and $(\text{CO})_3$ π^* orbitals with Cr ($d_{x^2-y^2, xy}$). The $16e$ orbitals are essentially from benzene e π

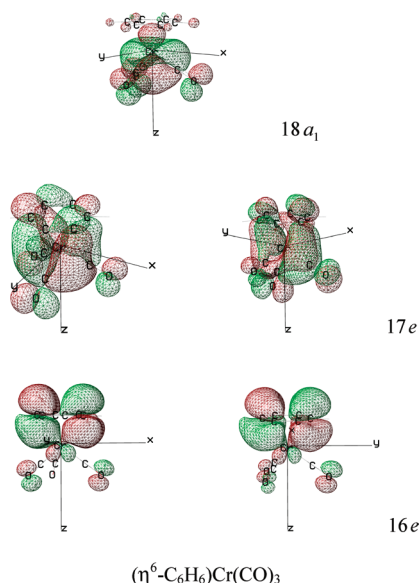


Figure 2. Plots of the frontier filled MOs for $(\eta^6\text{-C}_6\text{H}_6)\text{Cr}(\text{CO})_3$. The isosurface values are chosen to be 0.02 for all the MO plots.

orbitals. As for $(\eta^5\text{-C}_5\text{H}_5)\text{Mn}(\text{CO})_3$, it has 33 a' and 18 a'' occupied MOs. The HOMO 33 a' results from the mixing of Mn ($d_{x^2-y^2}$) with $(\text{CO})_3 \pi^*$. The 18 a'' and 32 a' orbitals result from the mixing of Mn (d_{xy}) and Mn (d_z) with $(\text{CO})_3 \pi^*$ orbitals, respectively. The 17 a'' and 31 a' orbitals are essentially from the mixing of Cp π orbitals with Mn (d_{xz}) and Mn (d_{yz}), respectively.

Table 2 lists the calculated IPs using the representative results of A1, B1, and C1 basis sets for $(\eta^4\text{-C}_4\text{H}_6)\text{Fe}(\text{CO})_3$ and $(\eta^5\text{-C}_5\text{H}_5)\text{Co}(\text{CO})_2$ along with the experimental values. For $(\eta^4\text{-C}_4\text{H}_6)\text{Fe}(\text{CO})_3$, the increasing order of IPs of filled MOs is $a' < a' \approx a'' < a' < a'' < a'$ for all methods. For $(\eta^5\text{-C}_5\text{H}_5)\text{Co}(\text{CO})_2$, the increasing orders of IPs of filled MOs are $a' < a' < a'' < a' < a' < a''$ for KB and $a' < a' < a'' < a'' < a' < a'$ for KT calculations, respectively. According to Table 2, the calculated IPs using the $\text{KB}^{\text{PBEPBE}}$ method are in good agreement with the experimental values. The range of errors as compared with experimental values is within 0.2 eV. For the KT calculations, the errors for IPs are 0.25–0.30, 0.30–0.51, and 1.03–1.27 eV for the $\text{KT}^{\text{CAM-B3LYP}}$, $\text{KT}^{\text{wB97XD}}$, and $\text{KT}^{\text{LC-wPBE}}$ methods, respectively. If the $\text{X}\alpha$ method is used for $(\eta^5\text{-C}_5\text{H}_5)\text{Co}(\text{CO})_2$, the first IP is due to ionization from the a'' orbital. It is clear

that the $\text{KB}^{\text{PBEPBE}}$ approach so far has the best prediction in IPs. One of the main reasons why the order of KS PBEPBE orbital energies is likely to be correct is because the present approach contains exchange-correlation potential.⁴²

Figure 3 shows the correlation diagrams of the frontier MOs of $(\eta^4\text{-C}_4\text{H}_6)\text{Fe}(\text{CO})_3$ and $(\eta^5\text{-C}_5\text{H}_5)\text{Co}(\text{CO})_2$. Similar to $(\eta^5\text{-C}_5\text{H}_5)\text{Mn}(\text{CO})_3$, the 3d orbitals of metals yield a' ($d_{x^2-y^2}$), a' ($d_{x^2-y^2}$), a' (d_{yz}), a'' (d_{xy}), and a'' (d_{xz}) orbitals. The π^* orbitals of $(\text{CO})_3$ are of a' , a' , a'' , a' , a'' , and a'' symmetries, and those of $(\text{CO})_2$ are of a' , a' , a'' , and a'' symmetries. The π^* orbitals of $(\eta^4\text{-C}_4\text{H}_6)$ and Cp are both of a' and a'' symmetries. There are 31 a' and 18 a'' occupied MOs for $(\eta^4\text{-C}_4\text{H}_6)\text{Fe}(\text{CO})_3$, and 28 a' and 17 a'' occupied MOs for $(\eta^5\text{-C}_5\text{H}_5)\text{Co}(\text{CO})_2$. According to our analysis of the nature of orbitals for $(\eta^4\text{-C}_4\text{H}_6)\text{Fe}(\text{CO})_3$, the HOMO (31 a') results from Fe ($d_{x^2-y^2}$) mixed with $(\eta^4\text{-C}_4\text{H}_6)(\text{CO})_3 \pi^*$. The 30 a' orbital is essentially from Fe ($d_{x^2-y^2}$) and $(\eta^4\text{-C}_4\text{H}_6)(\text{CO})_3 \pi^*$. MO 18 a'' results from Fe (d_{xy}) mixed with $(\eta^4\text{-C}_4\text{H}_6)(\text{CO})_3 \pi^*$, and MO 29 a' results from Fe (d_{yz}) mixed with $(\eta^4\text{-C}_4\text{H}_6)(\text{CO})_3 \pi^*$. The 17 a'' orbital is mainly from $(\eta^4\text{-C}_4\text{H}_6) \pi$ and Fe (d_{xz}). MO 28 a' is mainly from $(\eta^4\text{-C}_4\text{H}_6) \pi$. As for $(\eta^5\text{-C}_5\text{H}_5)\text{Co}(\text{CO})_2$, the 28 a' orbital results from $(\text{CO})_2 \pi^*$ mixed with Co (d_{yz}). The 27 a' orbital is essentially from the Co ($d_{x^2-y^2}$) orbital. The 17 a'' and 26 a' orbitals are mainly from Co (d_{xz}) and Co ($d_{x^2-y^2}$) mixed with $(\text{CO})_2 \pi^*$ orbitals, respectively. The 25 a' orbital corresponds to the π -bonding interaction between Cp π and Co (d_{yz}) orbitals, and 16 a'' corresponds to the π -bonding interaction between Cp π and Co (d_{xz}) orbitals. The 24 a' orbital is mainly from Cp π .

For the temporary anion shape resonance, we perform S-KB calculations on the unfilled orbitals to distinguish them from the ODC solutions for α between 0.0 and 3.0 via the PBEPBE ($\text{S-KB}^{\text{PBEPBE}}$), and then the S-KT calculations via CAM-B3LYP, wB97XD, and LC-wPBE ($\text{S-KT}^{\text{CAM-B3LYP}}$, $\text{S-KT}^{\text{wB97XD}}$, and $\text{S-KT}^{\text{LC-wPBE}}$) methods. First, we will present the results of $\text{S-KB}^{\text{PBEPBE}}$ for $(\eta^6\text{-C}_6\text{H}_6)\text{Cr}(\text{CO})_3$ and $(\eta^5\text{-C}_5\text{H}_5)\text{Mn}(\text{CO})_3$. Figure 4a shows the energies of the discretized continuum (DC)^{19–23,43} solutions as a function of the scale factor α for the e, a_1 , and a_2 virtual orbitals of $(\eta^6\text{-C}_6\text{H}_6)\text{Cr}(\text{CO})_3$ using the basis set A1 located at the appropriate nuclear positions. The energies of the DC solutions are obtained by solving the Kohn–Sham equation for a single electron in the absence of any potential. The stabilization graphs of the energies as a function of α for the e, a_1 , and a_2 virtual states of $(\eta^6\text{-C}_6\text{H}_6)\text{Cr}(\text{CO})_3$ using basis set A1 for the $\text{S-KB}^{\text{PBEPBE}}$ calculations are shown in Figure 4b.

TABLE 2: Calculated IPs (eV) for $(\eta^4\text{-C}_4\text{H}_6)\text{Fe}(\text{CO})_3$ and $(\eta^5\text{-C}_5\text{H}_5)\text{Co}(\text{CO})_2$

method	basis set	$(\eta^4\text{-C}_4\text{H}_6)\text{Fe}(\text{CO})_3$							$(\eta^5\text{-C}_5\text{H}_5)\text{Co}(\text{CO})_2$						
		a'	a'	a''	a'	a''	a'	d^b/eV	a'	a'	a''	a'	a'	a''	d^b/eV
$\text{KB}^{\text{PBEPBE}}$	A1	8.13	8.58	8.66	8.84	9.73	11.04	0.24	7.54	7.66	8.41	9.37	9.87	9.97	0.12
	B1	8.28	8.75	8.83	9.00	9.83	11.09	0.13	7.63	7.74	8.52	9.48	9.91	10.00	0.10
	C1	8.26	8.73	8.81	8.99	9.80	11.06	0.14	7.65	7.76	8.53	9.48	9.91	9.99	0.10
$\text{KT}^{\text{CAM-B3LYP}}$	A1	7.77	8.61	8.76	9.15	9.39	11.05	0.30	7.10	8.15	8.73	9.64	9.78	9.28	0.29
	B1	7.95	8.83	8.98	9.38	9.54	11.16	0.25	7.25	8.28	8.90	9.76	9.95	9.39	0.25
	C1	7.94	8.83	8.98	9.38	9.53	11.13	0.26	7.27	8.29	8.92	9.77	9.95	9.38	0.25
$\text{KT}^{\text{wB97XD}}$	A1	8.36	9.18	9.34	9.72	9.98	11.63	0.30	7.66	8.69	9.28	10.22	10.35	9.88	0.42
	B1	8.48	9.34	9.49	9.89	10.07	11.68	0.42	7.77	8.77	9.40	10.30	10.46	9.94	0.51
	C1	8.45	9.32	9.48	9.87	10.05	11.64	0.40	7.78	8.77	9.41	10.30	10.44	9.93	0.51
$\text{KT}^{\text{LC-wPBE}}$	A1	9.07	9.86	10.01	10.32	10.76	12.55	1.03	8.35	9.44	10.01	10.98	11.06	10.69	1.16
	B1	9.21	10.05	10.19	10.51	10.86	12.61	1.17	8.47	9.52	10.15	11.12	11.15	10.76	1.27
	C1	9.18	10.03	10.18	10.50	10.83	12.55	1.14	8.48	9.52	10.15	11.10	11.13	10.73	1.26
$\text{X}\alpha^a$		7.7	8.4	8.5	8.8	9.8	11.7	0.31	7.7 ^c	8.5	9.5	8.9	9.8	10.2	0.21
expt ^a		8.23	8.82	9.09	9.93	11.52			7.59	7.95	8.51	9.41	9.87	10.23	

^a The IPs are obtained from previous studies.²⁸ ^b Here d denotes the mean error relative to experimental IP data. ^c Value for a'' .

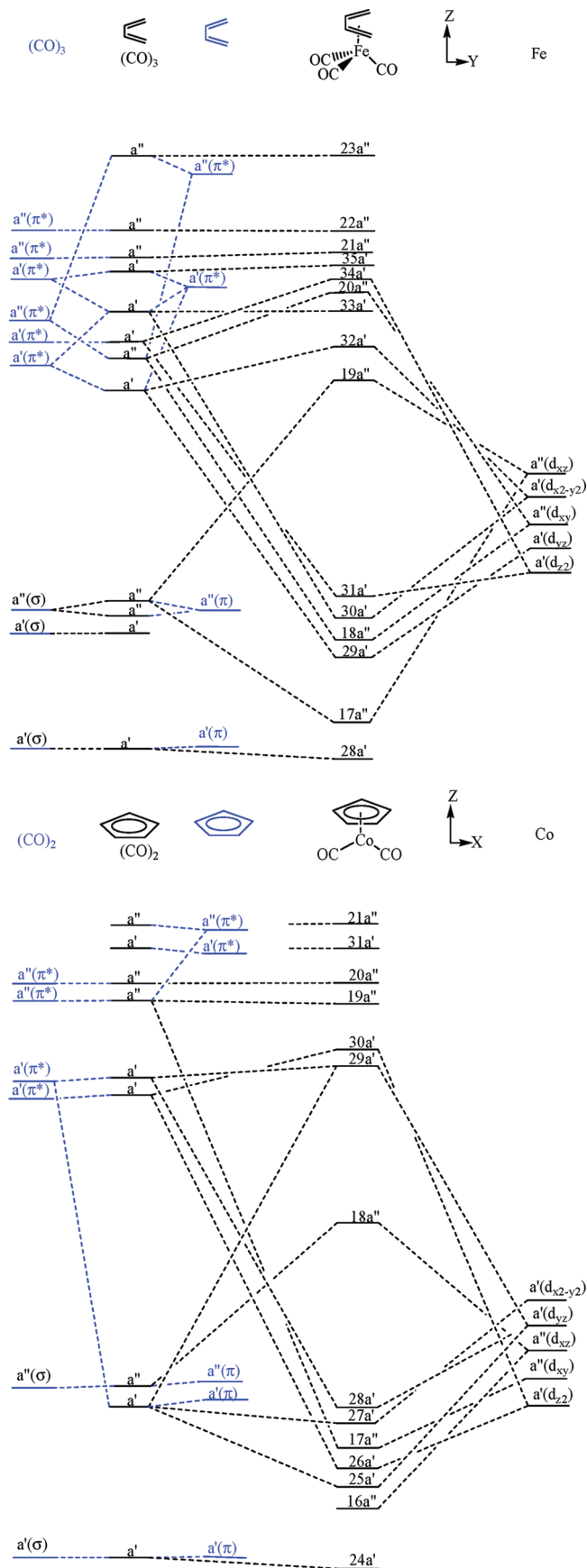


Figure 3. Correlation diagram of the frontier MOs for $(\eta^4\text{-C}_4\text{H}_6)\text{Fe}(\text{CO})_3$ and $(\eta^5\text{-C}_5\text{H}_5)\text{Co}(\text{CO})_2$.

There are two types of energies for virtual orbital solutions in the S-KB calculations. One is the unfilled orbital solution

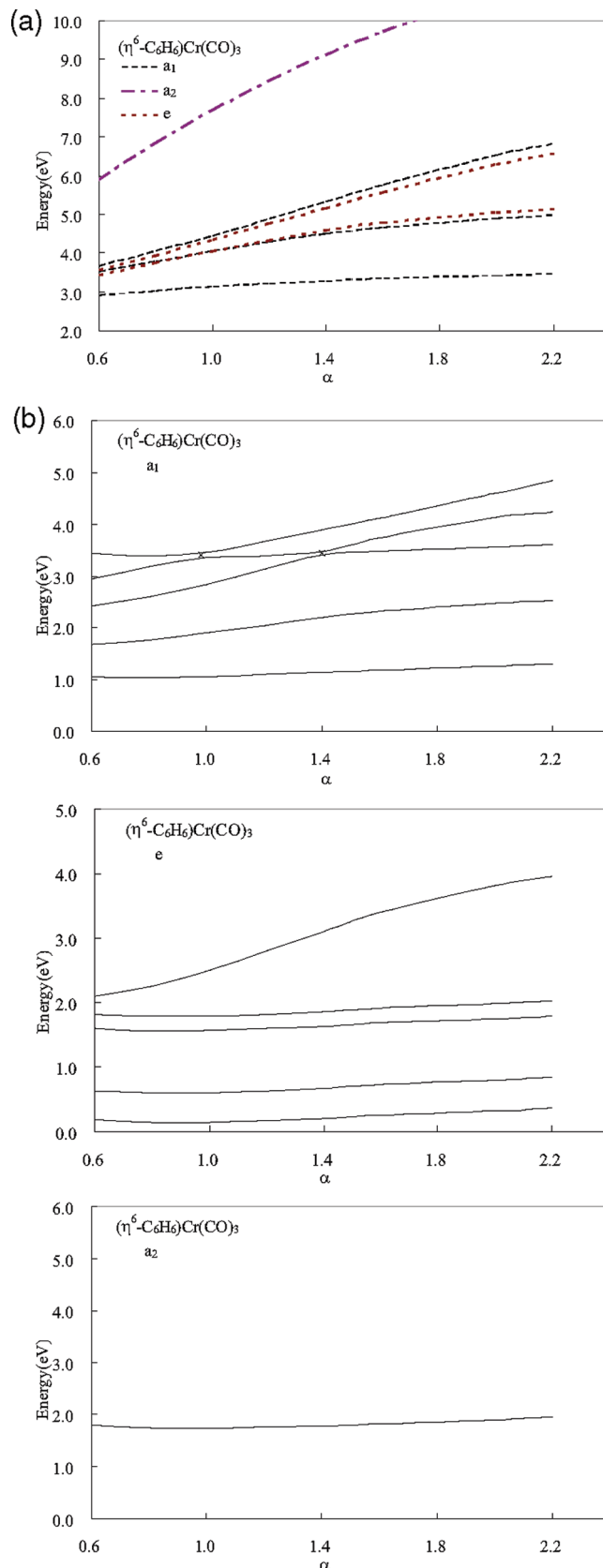


Figure 4. (a) Energies of e , a_1 , and a_2 virtual orbitals of $(\eta^6\text{-C}_6\text{H}_6)\text{Cr}(\text{CO})_3$ as a function of the scaling factor α for a free electron in the absence of potentials. (b) Stabilization graphs for $(\eta^6\text{-C}_6\text{H}_6)\text{Cr}(\text{CO})_3$ via S-KB^{TBGG} method. Energies of e , a_1 , and a_2 virtual orbitals as a function of α . The location of α_{ac} is marked with \times .

and the other is the ODC virtual orbital solution. The unfilled orbital solution and the ODC solutions are readily distinguished

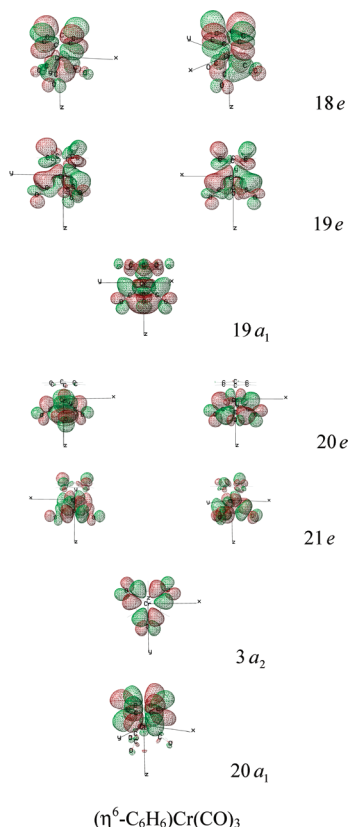


Figure 5. Plots of the frontier unfilled MOs at $\alpha = 2.0$ for $(\eta^6\text{-C}_6\text{H}_6)\text{Cr}(\text{CO})_3$. The isosurface values are chosen to be 0.02 for all the MO plots.

by examining how their energies vary with α . As shown in Figure 4b for the a_1 virtual orbitals, the first solution which remains stabilized with α is the $19a_1$ orbital solution and the stabilized energy value is 1.14 eV.⁴⁴ The second solution corresponds to the first ODC solution. The avoided crossings at $\alpha_{ac} = 1.0$ and 1.4 are due to the coupling between the $20a_1$ orbital solution with the second and third ODC solutions. The energies of the $20a_1$ orbital can be extracted from each two-state avoided crossing region. From Figure 4b, the energy values of the $20a_1$ orbital are both 3.40 eV at $\alpha_{ac} = 1.0$ and 1.4. Thus, the energy of the $20a_1$ orbital is 3.40 eV. As for the e virtual orbitals, the first to fourth solutions which remain stabilized with α are the 18e, 19e, 20e, and 21e orbital solutions and their stabilized energy values are 0.19, 0.65, 1.61, and 1.84 eV, respectively. The next four solutions correspond to the ODC solutions. For the a_2 virtual orbital, the first solution is the $3a_2$ orbital solution and the stabilized energy value is 1.79 eV.

In Figure 5, the first and third a_1 virtual orbitals, the first to fourth e virtual orbitals, and the first a_2 virtual orbital that correspond to the resonance solutions of $(\eta^6\text{-C}_6\text{H}_6)\text{Cr}(\text{CO})_3$ for $\alpha = 2.0$ are displayed. As can be seen in Figures 1 and 5, the 18e orbitals essentially result from $\text{Bz}(\text{CO})_3$ π^* orbitals. The 19e orbitals result from the π -antibonding interaction between $\text{Bz}(\text{CO})_3$ π orbitals and Cr (d_{xz} , d_{yz}). The 20e orbitals are essentially derived from the $\text{Bz}(\text{CO})_3$ π^* orbitals. The $19a_1$ orbital results from the antibonding interaction between $\text{Bz}(\text{CO})_3$ π^* orbitals and Cr (d_{z^2}). The 21e orbitals result from the antibonding interaction between $\text{Bz}(\text{CO})_3$ π^* orbitals and Cr ($d_{x^2-y^2}$, d_{xy}). The $3a_2$ and 22e orbitals are mainly from the $\text{Bz}(\text{CO})_3$ π^* orbitals. The $20a_1$ orbital is essentially from the benzene π^* .

Next, for $(\eta^5\text{-C}_5\text{H}_5)\text{Mn}(\text{CO})_3$, the stabilization graphs of the energies as a function of α for the a' and a'' virtual states using

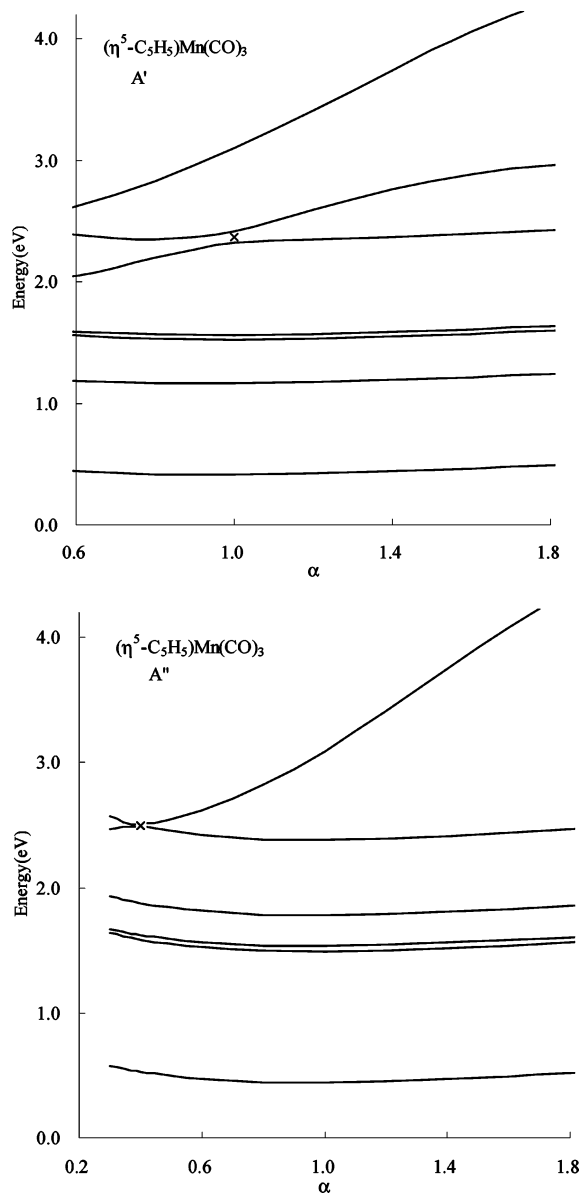


Figure 6. Stabilization graphs for $(\eta^5\text{-C}_5\text{H}_5)\text{Mn}(\text{CO})_3$ via S-KB^{PBEPBE} method. Energies of a' and a'' virtual orbitals as a function of α . The location of α_{ac} is marked with \times .

basis set A1 are shown in Figure 6. As shown in Figure 6, the first to fourth solutions which remain stabilized with α are the $34a'$, $35a'$, $36a'$, and $37a'$ orbital solutions and their stabilized energy values are 0.44, 1.19, 1.55, and 1.58 eV, respectively. The avoided crossing at $\alpha_{ac} = 1.0$ is due to the coupling between the fifth a' ($38a'$) unfilled orbital solution and first ODC solution. In Figure 6, the energy value of $38a'$ orbital is 2.37 eV at $\alpha_{ac} = 1.0$. The seventh solution corresponds to the second ODC solution. For the a'' virtual states, the first to fourth solutions which remain stabilized with α are the $19a''$, $20a''$, $21a''$, and $22a''$ orbital solutions and their stabilized energy values are 0.47, 1.51, 1.56, and 1.81 eV, respectively. The avoided crossing at $\alpha_{ac} = 0.4$ is due to the coupling between the $23a''$ orbital solution and the first ODC solution. The energy value of the $23a''$ orbital is 2.50 eV at $\alpha_{ac} = 0.4$. According to Figures 1 and 6, the LUMO $34a'$ corresponds to the antibonding interaction between $\text{Cp}(\text{CO})_3$ π^* orbitals and Mn (d_{yz}). The $19a''$ orbital corresponds to the antibonding interaction between $\text{Cp}(\text{CO})_3$ π^* orbitals and Mn (d_{xz}). The $35a'$ orbital is essentially from $(\text{CO})_3$ π^* orbitals and Mn (d_{z^2}). The $20\text{--}22a''$ orbitals are essentially from $(\text{CO})_3$

TABLE 3: Calculated AEs^a (eV) for (η^6 -C₆H₆)Cr(CO)₃ and (η^5 -C₅H₅)Mn(CO)₃ via S-KB^{PBEPBE} Method

	basis set									X α^b	expt ^b	
	A1	A2	A3	B1	B2	B4	C1	C2	C4			
(η ⁶ -C ₆ H ₆)Cr(CO) ₃												
a ₁	3.40	3.51	3.52	3.52	3.51	3.58	3.55	3.56	3.54	a ₂	3.2	3.63
e	1.84	1.84	1.93	2.10	2.06	2.09	2.08	2.08	2.08	a ₂	1.9	2.4
a ₂	1.79	1.88	1.86	2.12	2.12	2.09	2.08	2.08	2.08	e	1.8	2.4
e	1.61	1.63	1.68	1.92	1.89	1.89	1.90	1.89	1.90	e	1.7	1.82
a ₁	1.14	1.14	1.21	1.28	1.25	1.26	1.27	1.27	1.27	a ₁	1.2	0.96
e	0.65	0.66	0.71	0.89	0.83	0.86	0.88	0.86	0.88	e	1.0	0.96
e	0.19	0.25	0.26	0.39	0.38	0.36	0.36	0.37	0.35	a ₁	0.9	c
										e	0.1	
										e	−0.1	
(η ⁵ -C ₅ H ₅)Mn(CO) ₃												
a''	2.50	2.46	2.26	2.38	2.40	2.37	2.34	2.34	2.33	a''	2.0	2.36
a'	2.37	2.38	2.16	2.33	2.35	2.32	2.29	2.29	2.28	a''	1.7	2.36
a''	1.81	1.83	1.64	1.94	1.94	1.92	1.92	1.91	1.90	a''	1.6	1.8
a'	1.58	1.61	1.43	1.69	1.68	1.67	1.69	1.68	1.67	a'	1.6	1.8
a''	1.56	1.57	1.40	1.67	1.66	1.65	1.67	1.65	1.65	a'	1.5	1.8
a'	1.55	1.57	1.39	1.66	1.66	1.63	1.65	1.64	1.63	a'	1.1	1.8
a''	1.51	1.56	1.36	1.62	1.63	1.59	1.62	1.61	1.59	a'	1.0	1.8
a'	1.19	1.20	1.03	1.26	1.26	1.25	1.27	1.26	1.26	a''	1.0	1.22
a''	0.47	0.48	0.29	0.49	0.46	0.47	0.49	0.48	0.48	a''	0.8	0.2
a'	0.44	0.45	0.27	0.46	0.44	0.44	0.47	0.45	0.45	a'	0.8	0.2
										a'	0.4	
										a''	0.2	
										a'	0.1	

^a The energies of the HOMO (ϵ_{HOMO}) in eq 4 are calculated for each value of α even though the variations of ϵ_{HOMO} values are within 0.1 eV. ^b The AEs are obtained from previous studies.²⁸ ^c The calculated energy value is outside the observed range.

TABLE 4: Calculated AEs^a (eV) for (η^4 -C₄H₆)Fe(CO)₃ and (η^5 -C₅H₅)Co(CO)₂ via S-KB^{PBEPBE} Method

	basis set ^a									X α^b	expt ^b	
	A1	A2	A3	B1	B2	B4	C1	C2	C4			
(η ⁴ -C ₄ H ₆)Fe(CO) ₃												
a''	2.24	2.27	2.21	2.17	2.20	2.15	2.12	2.11	2.09	a''	2.0	2.21
a''	1.48	1.50	1.44	1.62	1.66	1.60	1.59	1.58	1.55	a''	1.7	1.26
a''	1.27	1.30	1.24	1.39	1.43	1.36	1.38	1.36	1.34	a'	1.3	1.26
a'	1.26	1.27	1.22	1.37	1.41	1.35	1.35	1.32	1.30	a''	1.2	1.26
a''	1.18	1.17	1.15	1.28	1.29	1.27	1.27	1.22	1.23	a'	1.1	1.26
a'	1.20	1.19	1.17	1.26	1.26	1.24	1.25	1.21	1.22	a'	1.0	1.26
a'	0.85	0.84	0.81	0.92	0.93	0.90	0.91	0.87	0.87	a''	1.0	1.26
a'	0.67	0.66	0.64	0.66	0.65	0.64	0.64	0.59	0.60	a''	0.8	c
a''	0.34	0.31	0.29	0.31	0.27	0.29	0.30	0.23	0.27	a'	0.1	c
										a''	0.0	
										a'	0.0	
										a'	-0.2	
(η ⁵ -C ₅ H ₅)Co(CO) ₂												
a''	2.62	2.63	2.61	2.49	2.51	2.48	2.45	2.45	2.39	a''	1.7	2.05
a'	2.58	2.58	2.64	2.50	2.52	2.48	2.45	2.45	2.40	a'	1.6	2.05
a''	1.78	1.72	1.76	1.87	1.85	1.84	1.87	1.83	1.81	a'	1.5	2.05
a''	1.72	1.64	1.70	1.79	1.75	1.77	1.79	1.74	1.73	a'	1.0	2.05
a'	1.02	0.93	0.99	1.06	1.02	1.04	1.06	1.02	1.01	a''	1.0	0.88
a'	0.97	0.89	0.95	0.99	0.95	0.96	0.98	0.94	0.92	a''	0.9	0.88
a''	0.00	-0.08	-0.04	-0.05	-0.12	-0.08	-0.05	-0.11	-0.10	a'	0.9	c
										a'	0.8	
										a'	0.0	

^a The energies of the HOMO (ϵ_{HOMO}) in eq 4 are calculated for each value of α even though the variations of ϵ_{HOMO} values are within 0.1 eV. ^b The AEs are obtained from previous studies.²⁸ ^c The calculated energy value is outside the observed range.

π^* . The 36a' and 37a' orbitals are mainly from the mixing of Mn (d_{xy}) and ($d_{x^2-y^2}$) with (CO)₃ π^* orbitals, respectively. The 38a' and 23a'' unfilled orbitals are derived from Cp π^* orbitals.

Table 3 illustrates the results of AEs using the S-KB methods for (η^6 -C₆H₆)Cr(CO)₃ and (η^5 -C₅H₅)Mn(CO)₃ along with the experimental values. The increasing orders of AEs of unfilled MOs are $e < e < a_1 < e < a_2 \approx e < a_1$ for (η^6 -C₆H₆)Cr(CO)₃ and $a' \approx a'' < a' < a'' \approx a' \approx a'' \approx a' < a'' <$

$a' \approx a''$ for (η^5 -C₅H₅)Mn(CO)₃. Notice that, if the X α method is used, the order of AEs is not conformable with ours. The additional anion states found in the X α calculations may represent ODC solutions. As can be seen from Table 3, the calculated AEs using the S-KB^{PBEPBE} methods are better than those using the X α method. One possible reason for the X α assignments to be worse is that it does not treat the σ and π orbitals on an equal footing when using the muffin-tin

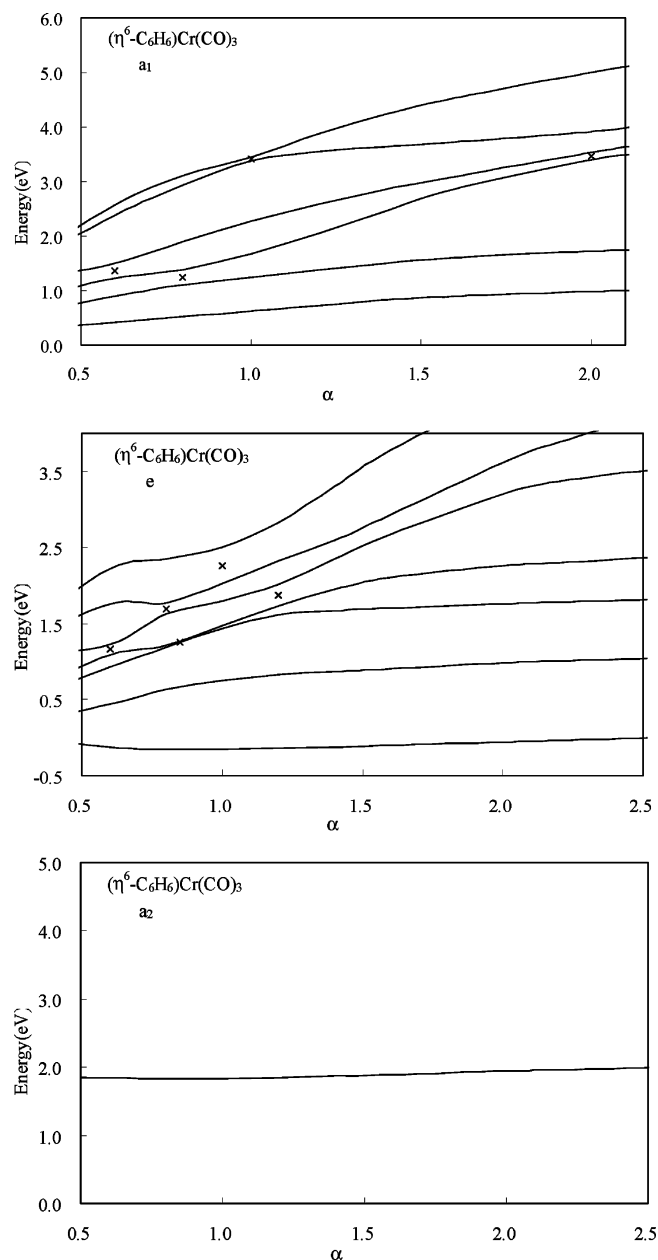


Figure 7. Stabilization graphs for $(\eta^6\text{-C}_6\text{H}_6)\text{Cr}(\text{CO})_3$ via S-KT^{CAM-B3LYP} method. Energies of e, a_1 , and a_2 virtual orbitals as a function of α . The location of α_{ac} is marked with x.

approximation (MTA). The AEs obtained are also quite sensitive to the sphere overlap used for MTA.

Our assignments for the shape resonance observed in the ET spectrum are slightly different from those of the X α method. According to our S-KB calculations for $(\eta^6\text{-C}_6\text{H}_6)\text{Cr}(\text{CO})_3$, the

3.63 eV feature in the ET spectrum is ascribed to electron capture into the empty $20a_1$ orbital. The resonances at 2.4 and 1.82 eV are associated with the capture into the $21e$, $3a_2$, and $20e$ orbitals. The resonance at 0.96 eV is associated with the capture into the $19e$ and $19a_1$ orbitals. The electron addition to $18e$ orbitals may not be observed in the ET spectrum. As for $(\eta^5\text{-C}_5\text{H}_5)\text{Mn}(\text{CO})_3$, the electron capture into the $38a'$ and $23a''$ orbitals corresponds to the resonance at 2.36 eV. The 1.8 eV feature can be ascribed to the electron capture into the $36a'$, $37a'$, and $20a''$ – $22a''$ orbitals. The capture into the $35a'$ orbital can be associated with the resonance at 1.22 eV. Finally, the electron addition to the $34a'$ and $19a''$ MOs can be associated with the resonance at 0.2 eV.

Table 4 lists the calculated AEs via the S-KB^{PBEPBE} method for $(\eta^5\text{-C}_4\text{H}_6)\text{Fe}(\text{CO})_3$ and $(\eta^4\text{-C}_5\text{H}_5)\text{Co}(\text{CO})_2$. As can be seen for $(\eta^5\text{-C}_4\text{H}_6)\text{Fe}(\text{CO})_3$, the increasing order of AEs of unfilled orbitals is $a'' < a' < a' \approx a'' \approx a'' < a'' < a''$. For $(\eta^5\text{-C}_5\text{H}_5)\text{Co}(\text{CO})_2$, the increasing order of AEs of unfilled orbitals is $a'' < a' \approx a' \approx a'' \approx a'' < a' \approx a''$. According to Tables 3 and 4, the calculated AEs are in good agreement with the experimental data. Both the inherent experimental errors for the ETS structures and the errors associated with determination of the resonance energies from the stabilization graphs could be as large as 0.1 eV.^{45,46} Consequently, the S-KB^{PBEPBE} calculations are able to yield accurate energies of temporary anion states of transition-metal carbonyls.

According to analysis of the nature of orbitals for $(\eta^4\text{-C}_4\text{H}_6)\text{Fe}(\text{CO})_3$, the LUMO ($19a''$) corresponds to the antibonding interaction between $(\eta^4\text{-C}_4\text{H}_6) \pi$ orbitals and Fe (d_{xz}). The $20a''$ orbital is mainly from $(\eta^4\text{-C}_4\text{H}_6)(\text{CO})_3$ $a'' \pi^*$ orbitals and Fe (d_{xy}). The $21a''$ and $22a''$ orbitals are essentially from $(\text{CO})_3$ $a'' \pi^*$. The $23a''$ orbital is derived from the $(\eta^4\text{-C}_4\text{H}_6) \pi^*$ orbital. Orbital $32a'$ is mainly from $(\eta^4\text{-C}_4\text{H}_6)(\text{CO})_3$ $a' \pi^*$ orbitals and Fe ($d_{x^2-y^2}$). The $33a'$ and $35a'$ orbitals are essentially from $(\eta^4\text{-C}_4\text{H}_6)(\text{CO})_3$ $a' \pi^*$ orbitals. The $34a'$ orbital is mainly from $(\eta^4\text{-C}_4\text{H}_6)(\text{CO})_3$ $a' \pi^*$ orbitals and Fe (d_z). For $(\eta^5\text{-C}_5\text{H}_5)\text{Co}(\text{CO})_2$, the $18a''$ orbital corresponds to the antibonding interaction between $(\eta^5\text{-C}_5\text{H}_5) \pi$ orbitals and Co (d_{xz}). The $29a'$ orbital corresponds to antibonding interaction between $(\eta^5\text{-C}_5\text{H}_5) \pi$ orbitals and Co (d_{yz}). Orbital $30a'$ is mainly from $(\text{CO})_2$ $a' \pi^*$ orbitals and Co (d_z). The $19a''$ and $20a''$ unfilled orbitals are essentially from $(\text{CO})_2$ $a'' \pi^*$. The $31a'$ and $21a''$ orbitals are derived from Cp π^* orbitals.

For the S-KT calculations, the stabilization graphs of the energies as a function of α for the e, a_1 , and a_2 virtual states of $(\eta^6\text{-C}_6\text{H}_6)\text{Cr}(\text{CO})_3$ via the S-KT^{CAM-B3LYP} method using the A1 basis set are shown in Figure 7. The obtained energy values of the $19a_1$ orbital are 1.36 eV at $\alpha_{ac} = 0.6$ and 1.25 eV at $\alpha_{ac} = 0.8$. The energy values of the $20a_1$ orbital are 3.42 eV at $\alpha_{ac} = 1.0$ and 3.47 eV at $\alpha_{ac} = 2.0$. The lowest value from each set will be defined as the energy of the temporary anion state.²⁶ Thus, the energies of the $19a_1$ and $20a_1$ orbitals are 1.25 and

TABLE 5: Calculated AEs (eV) for $(\eta^6\text{-C}_6\text{H}_6)\text{Cr}(\text{CO})_3$ via S-KT Methods for Basis Sets A1, B1, and C1

	S-KT ^{CAM-B3LYP}			S-KT ^{wB97XD}			S-KT ^{LC-wPBE}			expt ^a
	A1	B1	C1	A1	B1	C1	A1	B1	C1	
a_1	3.42	3.59	3.55	3.94	4.00	3.90	4.56	4.35	4.57	3.63
e	2.26	2.56	2.71	3.01	3.15	3.16	3.76	3.78	3.76	2.4
a_2	1.94	2.05	2.02	2.52	2.58	2.62	3.17	3.15	3.19	1.82
e	1.69	1.89	1.95	2.36	2.57	2.54	3.03	3.16	3.22	
a_1	1.25	1.19	1.21	1.98	2.00	2.00	2.48	2.44	2.61	0.96
e	1.16	1.10	1.19	1.64	1.81	1.77	2.23	2.40	2.38	
e	−0.06	−0.07	−0.10	0.54	0.58	0.57	0.97	0.88	0.92	

^a The AEs are obtained from previous studies.²⁸

TABLE 6: Calculated AEs (eV) for $(\eta^5\text{-C}_5\text{H}_5)\text{Mn}(\text{CO})_3$, $(\eta^4\text{-C}_4\text{H}_6)\text{Fe}(\text{CO})_3$, and $(\eta^5\text{-C}_5\text{H}_5)\text{Co}(\text{CO})_2$ via S-KT Methods

	method			expt ^a
	S-KT ^{CAM-B3LYP}	S-KT ^{wB97XD}	S-KT ^{LC-wPBE}	
$(\eta^5\text{-C}_5\text{H}_5)\text{Mn}(\text{CO})_3$				
a''	2.09	2.73	3.32	2.36
a'	2.07	2.77	3.22	
a''	1.41	2.01	2.53	1.8
a'	1.30	1.82	2.46	1.22
a''	1.29	1.89	2.40	
a'	1.06	1.69	2.31	
a''	1.04	1.69	2.30	
a'	0.54	1.14	1.81	0.2
a''	0.28	0.95	1.41	
a'	0.26	0.94	1.29	
$(\eta^4\text{-C}_4\text{H}_6)\text{Fe}(\text{CO})_3$				
a''	2.00	2.68	3.21	2.21
a''	1.12	1.77	2.33	1.26
a''	1.06	1.73	2.11	
a'	0.89	1.62	2.18	
a''	0.66	1.24	1.96	
a'	0.81	1.50	2.08	
a'	0.29	0.96	1.57	
a'	0.21	0.90	1.42	
a''	0.34	1.04	1.48	
$(\eta^5\text{-C}_5\text{H}_5)\text{Co}(\text{CO})_2$				
a''	2.19	2.80	3.38	2.05
a'	2.13	2.74	3.35	
a''	1.39	2.06	2.54	
a''	0.99	1.68	2.07	0.88
a'	0.31	0.98	1.60	
a'	0.16	0.76	1.32	
a''	-0.07	0.64	0.93	

^a The AEs are obtained from previous studies.²⁸

3.42 eV, respectively. As for the e virtual orbitals, the stabilized energy value for the 18e orbital is -0.06 eV. The energy values of the 19e orbitals are 1.16 eV at $\alpha_{\text{ac}} = 0.6$ and 1.27 eV at $\alpha_{\text{ac}} = 0.9$, respectively. The energy values of the 20e orbitals are 1.69 eV at $\alpha_{\text{ac}} = 0.8$ and 1.87 eV at $\alpha_{\text{ac}} = 1.2$, respectively. Accordingly, the energies of the 19e and 20e anion states are 1.16 and 1.69 eV, respectively. The energy value for the 21e orbitals is 2.26 eV at $\alpha_{\text{ac}} = 1.0$. For the a_2 virtual orbitals, the stabilized energy value for the $3a_2$ virtual orbital is 1.94 eV.

The calculated AEs of $(\eta^6\text{-C}_6\text{H}_6)\text{Cr}(\text{CO})_3$ for various S-KT via CAM-B3LYP, wB97XD, and LC-wPBE methods are summarized in Table 5. The S-KT^{LC-wPBE} and S-KT^{wB97XD} approaches overestimate AEs when compared with the experimental values. The AEs obtained from the S-KT^{LC-wPBE} and S-KT^{wB97XD} methods are larger than those obtained from the S-KT^{CAM-B3LYP} method (about 0.4 and 0.9 eV). Table 6 illustrates the calculated AEs of S-KT^{CAM-B3LYP}, S-KT^{wB97XD}, and S-KT^{LC-wPBE} approaches using the representative A1 basis set for $(\eta^5\text{-C}_5\text{H}_5)\text{Mn}(\text{CO})_3$, $(\eta^4\text{-C}_4\text{H}_6)\text{Fe}(\text{CO})_3$, and $(\eta^5\text{-C}_5\text{H}_5)\text{Co}(\text{CO})_2$. In Table 6, the calculated AEs using the S-KT^{CAM-B3LYP} method are in good agreement with the experimental values for three carbonyls. Nevertheless, the S-KT^{LC-wPBE} and S-KT^{wB97XD} approaches overestimate AEs when compared with the experimental values. The AEs obtained from the S-KT^{wB97XD} and S-KT^{LC-wPBE} methods are larger than those obtained from the S-KT^{CAM-B3LYP} method (about 0.7 and 1.2 eV). Possible reasons for the discrepancy are due to the different considerations of the exchange-correlation potential, self-interaction effect, and Coulomb contributions at large electron-molecule distance among these methods.^{47,48} For instance, the LC-wPBE functional may be overcorrected by inclusion of a too large

fraction of HF exchange, and the wB97XD functional may suffer from some self-interaction at short range. On the other hand, in the method of CAM-B3LYP, two extra parameters are used in the range separated Coulomb operator. To sum up, as compared with experimental values in Tables 3–6, the S-KT^{CAM-B3LYP} and S-KB^{PBEPBE} methods generally yield better AEs than those of the S-KT^{wB97XD} and S-KB^{LC-wPBE} methods for the transition-metal carbonyls.

4. Conclusion

The energies of filled and unfilled orbitals in various transition-metal carbonyls have been systematically studied by various approaches. The present investigation has demonstrated that the KB^{PBEPBE} calculations can yield very accurate results for IPs. In addition, the S-KB^{PBEPBE} and S-KT^{CAM-B3LYP} methods can yield good energy results for temporary anion states. Hence, it is believed that these two methods can be very useful in the studies of temporary anion states for transition-metal complexes.

Acknowledgment. We would like to thank the reviewers for valuable comments during the revision process and the National Center for High-Performance Computing for the computational resources provided. This work was supported by the National Science Council of Republic of China under Grant NSC 98-2113-M029-005.

References and Notes

- (1) (a) Muetterties, E. L.; Bleeke, J. R.; Wucherer, E. J.; Albright, T. A. *Chem. Rev.* **1982**, 82, 499–525. (b) Albright, T. A. *Acc. Chem. Res.* **1982**, 15, 149–155.
- (2) Merlic, C. A.; Walsh, J. C.; Tantillo, D. J.; Houk, K. N. *J. Am. Chem. Soc.* **1999**, 121, 3596.
- (3) Seyferth, D. *Organometallics* **2003**, 22 (1), 2.
- (4) Frazier, C. C.; Harvey, M. A.; Cockeriam, M. P.; Hand, H. M.; Chauchard, E. A.; Lee, C. H. *J. Phys. Chem.* **1986**, 90, 5703.
- (5) Rabalais, J. W. *Principles of Ultraviolet Photoelectron Spectroscopy*; John Wiley and Sons: New York, 1977.
- (6) Sanche, L.; Schulz, G. J. *Phys. Rev. A* **1972**, 5, 1672.
- (7) Jordan, K. D.; Burrow, P. D. *Chem. Rev.* **1987**, 87, 557.
- (8) Gengeliczki, Z.; Pongor, C. I.; Sztáray, B. *Organometallics* **2006**, 25, 2553.
- (9) Koopmans, T. *Physica* **1934**, 1, 104.
- (10) Kohn, W.; Sham, L. J. *Phys. Rev. A* **1965**, 140, 1133.
- (11) Simons, J. *J. Phys. Chem. A* **2008**, 112, 6401.
- (12) Tozer, D. J.; De Proft, F. *J. Phys. Chem. A* **2005**, 109, 8923.
- (13) Tozer, D. J.; De Proft, F. *J. Chem. Phys.* **2007**, 127, 034108.
- (14) De Proft, F.; Sablon, N.; Tozer, D. J.; Geerlings, P. *Faraday Discuss.* **2007**, 135, 151.
- (15) Sablon, N.; De Proft, F.; Geerlings, P.; Tozer, D. J. *Phys. Chem. Chem. Phys.* **2007**, 9, 5880.
- (16) Teale, A. M.; De Proft, F.; Tozer, D. J. *J. Chem. Phys.* **2008**, 129, 044110.
- (17) Hajgató, B.; Deleuze, M. S.; Tozer, D. J.; De Proft, F. *J. Chem. Phys.* **2008**, 129, 084308.
- (18) Falcetta, M. F.; Jordan, K. D. *J. Phys. Chem.* **1990**, 94, 5666.
- (19) Falcetta, M. F.; Jordan, K. D. *J. Am. Chem. Soc.* **1991**, 113, 2903.
- (20) Burrow, P. D.; Howard, A. E.; Johnston, A. R.; Jordan, K. D. *J. Phys. Chem.* **1992**, 96, 7570.
- (21) Juang, C.-Y.; Chao, J. S.-Y. *J. Phys. Chem.* **1994**, 98, 13506.
- (22) Hazi, A. U.; Taylor, H. S. *Phys. Rev. A* **1970**, 1, 1109.
- (23) Taylor, H. S. *Adv. Chem. Phys.* **1970**, 18, 91.
- (24) Fels, M. F.; Hazi, A. U. *Phys. Rev. A* **1972**, 5, 1236.
- (25) Taylor, H. S.; Hazi, A. U. *Phys. Rev. A* **1976**, 14, 2071.
- (26) Cheng, H.-Y.; Shih, C.-C. *J. Phys. Chem. A* **2009**, 113, 1548.
- (27) Cheng, H.-Y.; Shih, C.-C.; Chang, J.-T. *J. Phys. Chem. A* **2009**, 113, 9551.
- (28) Modelli, A.; Distefano, G.; Guerra, M.; Jones, D. J. *Am. Chem. Soc.* **1987**, 109, 4440.
- (29) Wei, Y.-H.; Cheng, H.-Y. *J. Phys. Chem. A* **1998**, 102, 3560.
- (30) Wachters, A. J. H. *J. Chem. Phys.* **1970**, 52, 1033.
- (31) Rappe, A. K.; Smedley, T. A.; Goddard, W. A., III. *J. Phys. Chem.* **1981**, 85, 2607.
- (32) We use the simplest “midpoint method” adopted by Burrow et al. to extract resonance energy (ref 20).

- (33) Perdew, J. P.; Burke, K.; Ernzerhof, M. *Phys. Rev. Lett.* **1996**, *77*, 3865.
- (34) Yanai, T.; Tew, D. P.; Handy, N. C. *Chem. Phys. Lett.* **2004**, *393*, 51.
- (35) Chai, J.-D.; Head-Gordon, M. *Phys. Chem. Chem. Phys.* **2008**, *10*, 6615.
- (36) Vydrov, O. A.; Scuseria, G. E.; Perdew, J. P. *J. Chem. Phys.* **2007**, *126*, 154109.
- (37) Frisch, M. J.; Trucks, G. W.; Schlegel, H. B.; Scuseria, G. E.; Robb, M. A.; Cheeseman, J. R.; Scalmani, G.; Barone, V.; Mennucci, B.; Petersson, G. A.; Nakatsuji, H.; Caricato, M.; Li, X.; Hratchian, H. P.; Izmaylov, A. F.; Bloino, J.; Zheng, G.; Sonnenberg, J. L.; Hada, M.; Ehara, M.; Toyota, K.; Fukuda, R.; Hasegawa, J.; Ishida, M.; Nakajima, T.; Honda, Y.; Kitao, O.; Nakai, H.; Vreven, T.; Montgomery, J. A., Jr.; Peralta, J. E.; Ogliaro, F.; Bearpark, M.; Heyd, J. J.; Brothers, E.; Kudin, K. N.; Staroverov, V. N.; Kobayashi, R.; Normand, J.; Raghavachari, K.; Rendell, A.; Burant, J. C.; Iyengar, S. S.; Tomasi, J.; Cossi, M.; Rega, N.; Millam, J. M.; Klene, M.; Knox, J. E.; Cross, J. B.; Bakken, V.; Adamo, C.; Jaramillo, J.; Gomperts, R.; Stratmann, R. E.; Yazyev, O.; Austin, A. J.; Cammi, R.; Pomelli, C.; Ochterski, J. W.; Martin, R. L.; Morokuma, K.; Zakrzewski, V. G.; Voth, G. A.; Salvador, P.; Dannenberg, J. J.; Dapprich, S.; Daniels, A. D.; Farkas, O.; Foresman, J. B.; Ortiz, J. V.; Cioslowski, J.; Fox, D. J. *Gaussian 09*, revision A.02; Gaussian, Inc.: Wallingford, CT, 2009.
- (38) Simion, D. V.; Sorensen, T. S. *J. Am. Chem. Soc.* **1996**, *118*, 7345.
- (39) Berndt, A. F.; Marsh, R. F. *Acta Crystallogr.* **1963**, *16*, 118.
- (40) Byers, L. R.; Dahl, L. F. *Inorg. Chem.* **1980**, *19*, 277.
- (41) Burrow, P. D.; Modelli, A.; Guerra, M.; Jordan, K. D. *Chem. Phys. Lett.* **1985**, *118*, 328.
- (42) (a) Baerends, E. J.; Gritsenko, O. V. *J. Phys. Chem. A* **1997**, *101*, 5383. (b) Baerends, E. J. *Theor. Chem. Acc.* **2000**, *103*, 265. (c) Chong, D. P.; Gritsenko, O. V.; Baerends, E. J. *J. Chem. Phys.* **2002**, *116*, 1760.
- (43) Falcetta, M. F.; Chui, Y.; Jordan, K. D. *J. Phys. Chem. A* **2000**, *104*, 9605.
- (44) (a) When the energies of ODC solutions are much higher than those of the resonance states, no avoided crossings will be found in the stabilization graphs. (b) In typical stabilization graphs, the lowest states correspond to ODC solutions if basis sets with sufficiently low exponents are used in HF or post-HF methods. However, the lowest states are typically the resonance states when using the DFT method. The reasons for the discrepancy are perhaps caused by different considerations of exchange-correlation potential and self-interaction effect.
- (45) Jordan, K. D.; Michejda, J. A.; Burrow, P. D. *J. Am. Chem. Soc.* **1976**, *98*, 7189.
- (46) Chao, J. S.-Y.; Jordan, K. D. *J. Phys. Chem.* **1987**, *91*, 5578.
- (47) Vydrov, O. A.; Scuseria, G. E. *J. Chem. Phys.* **2005**, *122*, 184107.
- (48) Dutoi, A. D.; Head-Cordan, M. *Chem. Phys. Lett.* **2006**, *422*, 230.

JP9101674